Analytic Orbit Design for Observation of Earth Sites

Francesco de Dilectis*[1], Daniele Mortari[2]

Department of Aerospace Engineering, Texas A&M University
College Station, TX, U.S.A.

*[1]f.de.dilectis@tamu.edu; [2]mortari@tamu.edu

Abstract

Satellite observation of specific Earth sites or regions usually requires the use of compatible (resonant) orbits. If the observing sensor is optimized for a given altitude then the orbit must also be circular. This study provides analytical derivation of satellite ground tracks of *any* compatible circular orbits and for a full repetition cycle. The purpose is to offer equations whose solutions are *all* the points coordinates in which the ground track crosses itself, here called $\circledcirc$ -points. The geographical locations of these points along with the approximate expressions of the associated dwell times allow developing optimal orbit design for civilian or military satellite observation missions.

Keywords

Satellite Observation; Resonant Orbits; Repetitive Ground Tracks

Nomenclature

a= semi major axis [km]
e= eccentricity [-]
p=semi latus rectum [km]
i=inclination [rad]
Ω=right ascension of the ascending node [rad]
ω=anomaly of perigee [rad]
φ= true anomaly [rad]
n=mean motion [rad/s]
λ=latitude [rad]
β= longitude [rad]
T_p=orbital nodal period [s]
T_d=Greenwich nodal period [s]
J_2=Earth's second dynamic form factor [-]
$R_\oplus$ =Earth's radius [km]
$\omega_\oplus$ =Earth sidereal rotation rate [rad/s]
μ=Earth's gravitational constant [km^3/s^2]
C_x=cos x
S_x=sin x

Introduction

Observation by satellites on Earth's sites or regions is of interest for both civilian and military purposes. Space missions to monitor the values of physical quantities in specific geographical areas are of great interest for the scientific community while reconnaissance missions to perform persistent observation on sites, borders, or regions, are of high interest for intelligence and the defense community. Another important area of interest is satellite communications with specific Earth locations by single satellites or by satellite constellations.

Observation on Earth's sites or regions was also the focus of «Two-Way Orbits», from O. Abdelkhalic e D. Mortari, where the concept of ``two-ways'' orbits was introduced. The repeated ground track path of these orbits is a closed-loop trajectory that intersects itself, in some points, with tangent intersections. This allows designing orbits (and constellations) where the spacecraft passes over these tangent intersections once in a prograde and once in a retrograde mode and at different altitudes. The design of these orbits has been done by numerical optimization, specifically using Genetic Algorithms. Conversely, the focus of this paper is to find the *analytic expressions* of the intersection points of repeating ground-track trajectories (called X-points) as produced by circular orbits. Motivation is driven by the fact that the use of elliptical orbits is in contrast with the design of observing sensors, which is optimal for specific fixed altitude. The design of orbits that optimally and repeatedly observe Earth's sites implies the use of compatible orbits whose definition is summarized in the next subsection.

Compatible Orbits

To obtain optimal coverage of specific Earth's sites or regions, compatible orbits must be adopted. According to Carter, these are a set of orbits for which the ratio between the *orbit nodal period* (time between two subsequent equator crossings in ascending mode, T_p) and the *nodal period of Greenwich* (elapsed time for

Greenwich meridian between two subsequent crossings of the orbit ascending node line, T_d) is rational. Carter defined these orbits as

$$N_p T_p = N_p \frac{2\pi}{n+\dot{\omega}} = N_d T_d = N_d \frac{2\pi}{\omega_\oplus - \dot{\Omega}} \qquad (2.1)$$

where N_p and N_d are two integers representing the number of nodal periods completed by the satellite and the number of times that the Greenwich meridian crosses the orbit ascending node line in the repetition time (cycle), $T_{rep}=N_pT_p = N_dT_d$, respectively. The main gravitational perturbation has been taken into account in Equation (2.1) due to the Earth oblateness, known as the J_2 effect. The secular and persistent J_2 effect modifies the mean motion according to

$$n = n_0\left[1+\frac{3}{4}J_2\left(\frac{R_\oplus}{p}\right)^2(2-3\sin^2 i)\sqrt{1-e^2}\right], \qquad (2.2)$$

where $n_0 = \sqrt{\mu/a^3}$, the unperturbed mean motion, linearly changes the right ascension of the ascending node,

$$\dot{\Omega} = -\frac{3}{2}J_2\left(\frac{R_\oplus}{p}\right)^2 n\cos i, \qquad (2.3)$$

as well as the argument of perigee,

$$\dot{\omega} = \frac{3}{4}J_2\left(\frac{R_\oplus}{p}\right)^2 n(5\cos^2 i-1), \qquad (2.4)$$

while the remaining parameters (a, e and i) remain unchanged

$$\frac{da}{dt}\approx 0, \frac{de}{dt}\approx 0, \text{and}\ \frac{di}{dt}\approx 0.$$

In particular, for circular orbits (e = 0) the sum, $n + \omega$, assumes the value

$$n_c = n+\dot{\omega} = n_0[1+\xi(2-3\sin^2 i)][1+\xi(5\cos^2 i-1)]$$

$$\text{where} \qquad \xi = \frac{3}{4}J_2\left(\frac{R_\oplus}{R}\right)^2$$

However, by disregarding the ξ^2 term (for R = 8,000 km, $\xi \cong 5 \times 10^{-4}$), previous equation can be written as

$$n_c = n+\dot{\omega} \approx n_0[1-2\xi(1-4\cos^2 i)], \qquad (2.5)$$

which is an approximated expression for the modified mean motion of circular orbits.

The orbit nodal period as defined by Eq. (2.1) is correct for circular orbits only. For elliptical orbit the nodal period is also a function of the initial value of the argument of perigee, ω_0. However, the variation of the nodal period with ω_0 is very small (order of few seconds for LEO orbits) and therefore, Carter's definition, $T_P = 2\pi/(n+\dot{\omega})$ can be considered a good expression of the nodal period for small eccentric orbits. The rotation of the apsidal line affecting elliptical orbits complicates the definition of compatible orbits as the apsidal line rotation period must be synchronized with the orbit nodal period.

For assigned values of N_d, N_p, e, and i, Eq. (2.1) becomes a nonlinear equation in terms of the semi-major axis only. This nonlinear equation must be solved to obtain the compatible semi-major axis. This is done by rewriting Eq. (2.2), Eq. (2.3), and Eq. (2.4), in the following compact mode

$$n = \sqrt{\frac{\mu}{a^3}}\left(1+\frac{c_m}{a^2}\right), \qquad \dot{\Omega} = c_\Omega \frac{a^2+c_m}{a^4}\sqrt{\frac{\mu}{a^3}},$$
$$\dot{\omega} = c_\omega \frac{a^2+c_m}{a^4}\sqrt{\frac{\mu}{a^3}}, \qquad (2.6)$$

Where

$$\begin{cases} c_m &= \frac{3}{4}J_2\left(\frac{R_\oplus}{1-e^2}\right)^2(2-3\sin^2 i)\sqrt{1-e^2} \\ c_\Omega &= -\frac{3}{2}J_2\left(\frac{R_\oplus}{1-e^2}\right)^2\cos i \\ c_\omega &= \frac{3}{4}J_2\left(\frac{R_\oplus}{1-e^2}\right)^2(5\cos^2 i-1) \end{cases}$$

Substituting Eq (2.6) with Eq (2.1) and setting $c_n = N_p c_\Omega + N_d c_\omega$, the following function,

$$f(a) = N_p(\omega_\oplus - \dot{\Omega}) - \sqrt{\frac{\mu}{a^3}}\left(N_d+\frac{c_n}{a^2}\right)\left(1+\frac{c_m}{a^2}\right) = 0, \qquad (2.7)$$

is obtained. Equation (2.7) can be solved using Newton-Raphson iterative method, $a_{k+1} = a_k - \frac{f(a_k)}{f'(a_k)}$, where, by setting $c_0 = c_m N_d + c_n$, the derivative has the expression

$$f'(a) = \frac{n}{2a}\left(3N_d + 7\frac{c_0}{a^2} + 11\frac{c_m c_n}{a^4}\right),$$

and where the starting point a_0 can be chosen as the semi-major axis of a compatible unperturbed orbit

$$N_p\omega_\oplus = N_d n_0 \qquad \rightarrow \qquad a_0 = \sqrt[3]{\mu\left(\frac{N_d}{N_p\omega_\oplus}\right)^2} \qquad (2.8)$$

The report «Goddard Trajectory Determination Subsystem Mathematical Specifications», by Wagner presents an alternative iterative method to calculate the mean semi-major axis of a compatible orbit. The algorithm begins with the evaluation, as a starting point, of the unperturbed semi-major axis a_0, as in Eq. (2.8). Then, a is evaluated through the following iterative process

$$a_{k+1} = a_0\,\delta_k^{(1)}\,\delta_k^{(2)}$$

where

$$\begin{cases} \delta_k^{(1)} = \left[1+\frac{3}{4}J_2\left(\frac{R_\oplus}{a_k}\right)^2(2-3\sin^2 i)\right]^{2/3} \\ \delta_k^{(2)} = \left[1-\frac{3}{4}J_2\left(\frac{R_\oplus}{a_k}\right)^2\left(1+\frac{2N_p}{N_d}\cos i-5\cos^2 i\right)\right]^{2/3} \end{cases}$$

In order to obtain the equation of the ground track, the next subsection provides the trigonometric relationships relating the angles used to identify the position of a point on the Earth surface (geographical latitude, λ, and longitude, β), and the angular parameters used to define the position of the satellite in the inertial frame (inclination, i, and the anomaly from the node line, φ). These relationships are introduced and the ground track parametric equation is then derived.

Geometrical Relationships

Let us consider the ground track of a satellite in circular orbit with inclination i. Without losing generality, it can be assumed that the right ascension of ascending node is aligned with the first point of Aries (vernal axis), $\Omega = 0$, and the Greenwich meridian crosses the ascending node, $\alpha_G = 0$.

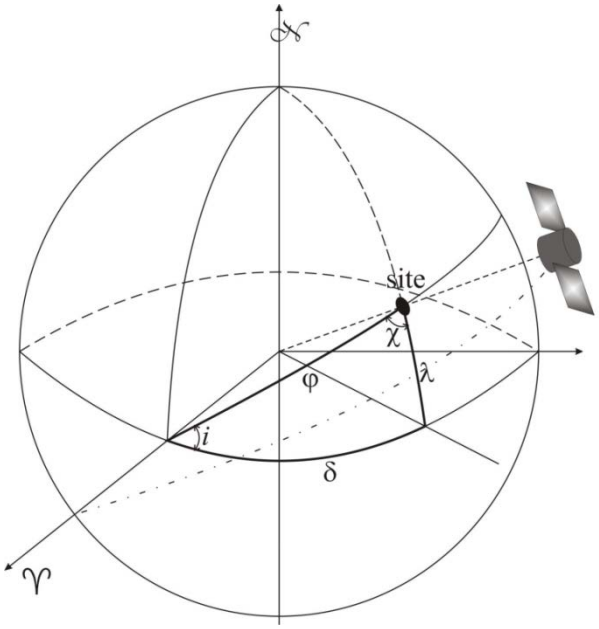

FIGURE 1 SATELLITE OBSERVATION GEOMETRY (ASCENDING MODE)

Under these assumptions, it can be seen from Fig. 1 that the angles involved for the ascending point (subscript "a") are δ_a, indicating the right ascension from the ϒ axis, λ, the geographical latitude of the sub-satellite point, and $\varphi = n_c t$, indicating the angle in the orbit plane from the sub-satellite point to the ascending node line. Among these angles, the following relationships hold

$$\begin{cases} \cos i = \sin\chi_a \cos\lambda \\ \cos\chi_a = \sin i \cos\delta_a \\ \tan\delta_a = \cos i \tan\phi_a \end{cases} \text{and} \begin{cases} \tan i \tan\chi_a = 1/\cos\phi_a \\ \sin\delta_a = \sin\chi_a \sin\phi_a \\ \sin i \sin\phi_a = \sin\lambda \end{cases} \quad (2.9)$$

All these relationships are just spherical trigonometry identities applied to the spherical triangle which is highlighted in Fig. 1. For the descending point (subscript "d"), which happen at the same latitude, the angles satisfy the following relationships

$$\lambda_d = \lambda_a,\ \phi_d = \pi - \phi_a,\ \delta_d = \pi - \delta_a,\ \chi_d = \pi - \chi_a.$$

Ground Track Equation

The parametric equations for the ground track can be obtained considering the unit vector identifying the sub-satellite point in the Earth-Centered Earth-Fixed (ECEF) reference frame, $\hat{\mathbf{s}}_E \triangleq \{\cos\lambda\cos\beta, \cos\lambda\sin\beta, \sin\lambda\}^T$, where λ and β indicate the sub-satellite point latitude and longitude, respectively. The position of the satellite in the Orbit Inertial frame is given by the unit vector $\hat{\mathbf{s}}_S \triangleq \{\cos n_c t, \sin n_c t, 0\}^T$. For circular orbit and disregarding the effect of Earth oblateness, the transformation matrix between these two reference frames is $R_3(\omega_\oplus t - \dot{\Omega})R_1(i)$, where R_1 and R_3 are the matrices performing rigid rotations about the first and third coordinate axis, respectively. Therefore, we can write

$$\begin{Bmatrix} C_\lambda C_\beta \\ C_\lambda S_\beta \\ S_\lambda \end{Bmatrix} = \begin{bmatrix} C_\alpha & S_\alpha & 0 \\ -S_\alpha & C_\alpha & 0 \\ 0 & 0 & 1 \end{bmatrix} \begin{bmatrix} 1 & 0 & 0 \\ 0 & C_i & S_i \\ 0 & -S_i & C_i \end{bmatrix} \begin{Bmatrix} C_{n_c t} \\ S_{n_c t} \\ 0 \end{Bmatrix}$$

where $\alpha = (\omega_\oplus - \dot{\Omega})t$ which leads to the following system of equations

$$\begin{cases} C_\lambda C_\beta = C_\alpha C_{n_c t} + S_\alpha C_i S_{n_c t} \\ C_\lambda S_\beta = C_\alpha C_i C_{n_c t} + S_\alpha S_{n_c t} \\ S_\lambda = S_i S_{n_c t} \end{cases}$$

that allows us to obtain the equations of the ground track

$$\begin{cases} \lambda(t) = \sin^{-1}[-S_i S_{n_c t}] \\ \beta(t) = \tan^{-1}\left\{\dfrac{C_\alpha C_{n_c t} + S_\alpha C_i S_{n_c t}}{C_\alpha C_i C_{n_c t} + S_\alpha S_{n_c t}}\right\} \end{cases}$$

Figure 2 shows, by setting $Np = 24$, $N_d = 7$, and $i = 55^o$, an example of the ground track trajectory for the repetition time $T_{\text{rep}} = N_p \dfrac{2\pi}{n_c} = N_d \dfrac{2\pi}{\omega_\oplus - \dot{\Omega}}$ in which two "elementary patterns," associated with the north and south hemisphere, respectively coloured in red and green are highlighted.

In addition to the obvious and expected symmetry with respect to the axes, several regularities are visible in the pattern of the ground track trajectory. In particular, for a given value of latitude, there are exactly N_P intersections, equally spaced in longitude. Similarly, for an assigned value of longitude, several

intersections at different latitudes occur. The two parameters ruling the intersection pattern are the radius (circular orbits) and the inclination. In the next subsection the conditions capable to evaluate the ground track intersections are given.

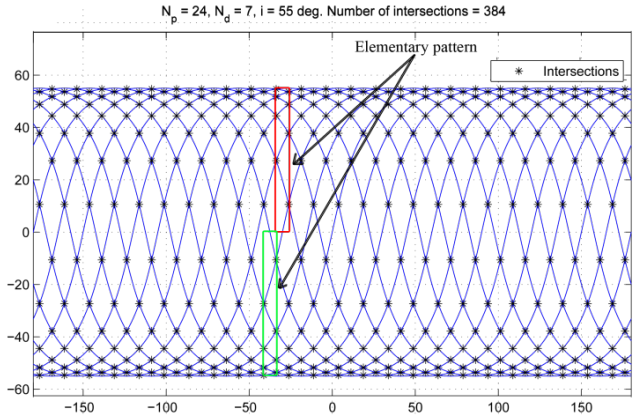

FIGURE 2 EXAMPLE OF SATELLITE GROUND TRACK INTERSECTIONS DURING A REPETITION PERIOD

Solving the Compatibility Condition

Let us consider a point where the ground track trajectory crosses a given latitude for two times, one when it ascends toward north and another time when it descends toward south. Let ΔT be the time difference between the time at which the satellite crosses that latitude in ascending mode and the time when it crosses again in descending mode. This time interval can be expressed in two different ways, using either Earth rotations

$$\Delta T = \frac{2\pi\alpha}{\omega_\oplus - \dot{\Omega}} + \frac{\delta_d - \delta_a}{\omega_\oplus - \dot{\Omega}} = \frac{2\pi\alpha}{\omega_\oplus - \dot{\Omega}} + \frac{\pi - 2\delta_a}{\omega_\oplus - \dot{\Omega}}, \quad \alpha \in \mathbb{Z}; \tag{3.1}$$

or orbit revolutions

$$\Delta T = \frac{2\pi\beta}{n_c} + \frac{\phi_d - \phi_a}{n_c} = \frac{2\pi\beta}{n_c} + \frac{\pi - 2\phi_a}{n_c}, \quad \beta \in \mathbb{Z}. \tag{3.2}$$

Both these equations account for an integer number of complete rotations or revolutions plus the exceeding angles $\delta_d+\delta_a$ or $\varphi_d+\varphi_a$. Employing Equating Eq. (3.1) and Eq. (3.2) as well as the compatibility equation for circular orbits, $N_p(\omega_\oplus - \dot{\Omega}) = N_d n_c$, we obtain

$$\frac{1}{\omega_\oplus - \dot{\Omega}}(2\pi\alpha + \pi - 2\delta_a) = \frac{1}{n_c}(2\pi\beta + \pi - 2\phi_a)$$

which can be written as

$$\alpha N_p \frac{2\pi}{N_d n_c} + N_p \frac{\pi - 2\delta_a}{N_d n_c} = \beta \frac{2\pi}{n_c} + \frac{\pi - 2\phi_a}{n_c}.$$

Using the third of Eq. (2.9) and considering that $\varphi_a = n_c t$, we obtain

$$\alpha N_p - \beta N_d + \frac{\pi - 2\tan^{-1}[\cos i \tan(n_c t)]}{2\pi} N_p - \frac{\pi - 2n_c t}{2\pi} N_d = \alpha N_p - \beta N_d + f(t) = 0. \tag{3.3}$$

The first two terms in Eq. (3.3) always add up to an integer. The last two instead can take any real value and can be indicated by a function of time $f(t)$. When f is an integer, then Eq. (3.3) becomes a Diophantine equation whose solutions identify intersections of the ground track trajectory. The analysis of the f function is the main focus of this study. Because of the symmetry, the analysis can be limited to the $n_c t \in \left[0, \frac{\pi}{2}\right]$ range.

Analysis of Function f

The purpose of our analysis is to find the times t at which the function f assumes integer values. The function is continuous in $n_c t$ and, because of the symmetry, the search can be limited to the $n_c t \in \left[0, \frac{\pi}{2}\right]$ range. Therefore, finding minimum and maximum values of f in the searching interval, called $[f_{min}, f_{max}]$, also provides the complete set of integers for f and associated times where the ground track intersects itself, i.e. $[\lceil f_{min} \rceil, \lfloor f_{max} \rfloor] \in \mathbb{Z}$, $\lceil \bullet \rceil$ and $\lfloor \bullet \rfloor$ indicate the "`floor`" and the "`ceil`" functions, respectively.

These extremal values may occur at the range limits ($n_c t = 0$ and $n_c t = \pi/2$) or inside the interval, in which case the first derivative f' can be used to find the locations of minumum/maximum (we will show later that f can have at most one internal stationary point). Since $f(0) = (N_p - N_d)/2$, there will be a set of intersections at the equator ($n_c t = 0$) whenever N_p and N_d are both odd (they cannot be both even as they must be coprime), so that their difference is even. As $n_c t$ approaches $\pi/2$, function f assumes different values depending on the sign of cos$i$ because

$$\lim_{x \to \frac{\pi}{2}} \tan^{-1}(\cos i \tan x) = \begin{cases} +\pi/2, & \text{if } \cos i > 0 \\ -\pi/2, & \text{if } \cos i < 0 \end{cases}$$

and, in particular, $f(\pi/2) = 0$ for prograde orbits and $f(\pi/2) = N_p$ for retrograde orbits.

The expression of the first derivative, f', is

$$\frac{\partial f}{\partial(n_c t)} = \frac{1}{\pi}\left[N_d - \frac{N_p \cos i}{\cos^2(n_c t) + \cos^2 i \sin^2(n_c t)}\right] \tag{3.4}$$

while the second derivative, f'', is

$$\frac{\partial^2 f}{\partial(n_c t)^2} = -\frac{N_p}{\pi}\left[\frac{\sin i}{\cos^2(n_c t) + \cos^2 i \sin^2(n_c t)}\right]^2 \cos i \sin(2n_c t). \tag{3.5}$$

Note that f'' is always negative for prograde orbits ($\cos i > 0$) and positive for retrograde orbits ($\cos i < 0$), which implies that f' is monotone in all cases, proving, as previously anticipated, that f can only have one internal stationary point (minimum or maximum). The analysis so far clearly shows how the inclination i plays a primary role in determining the behavior of f.

Its importance will be highlighted further in the discussion regarding the zeroes of f'.

By setting $f'' = 0$, we obtain

$$\sin^2(n_c t)\cos^2 i - \tau\cos i + \cos^2(n_c t) = 0, \quad (3.6)$$

where $\tau = N_p / N_d$,which can be reformulated in two different forms

$$\sin^2(n_c t) = \frac{1-\tau\cos i}{\sin^2 i} \quad (a)$$

$$\cos i = \frac{\tau - \sqrt{\tau^2 - \sin^2(2n_c t)}}{2\sin^2(n_c t)} \quad (b) \quad (3.7)$$

where the positive solution of Eq. (3.7b) is discarded as it gives values for cos$i$ outside the admissible range [-1,+1]. Equation (3.7a) enable to derive the limit values of inclination for which the derivative can vanish

$$\sin^2(n_c t) = 0 \rightarrow i_{\min} = \cos^{-1}\left(\frac{1}{\tau}\right)$$

$$\sin^2(n_c t) = 1 \rightarrow i_{\max} = \frac{\pi}{2} \quad (3.8)$$

Therefore, there is no maximum within the [$f(0)$, $f(\pi/2)$] range for orbits at $i < \cos^{-1}(1/\tau)$. Another way to obtain this result is by means of the note that $i < \cos^{-1}(1/\tau)$ is equivalent to $(N_p/N_d)\cos i > 1$. By rewriting Eq. (3.6) in the form $(\sin^2 i \cos^2(n_c t) + \cos^2 i) - (N_p/N_d)\cos i$, and since the terms in brackets cannot be greater than 1, it is concluded that the derivative assumes negative values at both extremes. Together with monotonicity, this proves the result.

In the following, we indicate $\cos^{-1}(1/\tau) = i_1^*$, and this inclination is called the first characteristic inclination. When $i = i_1^*$, the maximum is located exactly at $n_c t = 0$ with $f' = 0$. Orbits with inclinations $i < i_1^*$experience the maximum with $f' < 0$. Assuming the spacecraft at the ascending node at the initial time then f is a representation of the first quarter of a ground track. Consequently, an orbit inclined at the first characteristic inclination, i_1^*, crosses the equator along the local meridian. Whenever $N_p - N_d$ is even, subsequent ground tracks are also tangent to each other at the equator.

Alternatively, Eq. (3.7b) can be substituted into Eq. (3.5) to just obtain a function of $n_c t$

$$f^* = \frac{N_p - N_d}{2} + \frac{1}{\pi}\left[N_d n_c t - N_p \tan^{-1}\left(\frac{\tau - \sqrt{\tau^2 - \sin^2(2n_c t)}}{2\sin(2n_c t)}\right)\right]. \quad (3.9)$$

Equation (3.9) provides solutions (associated with $f^* \in \mathbb{Z}$) of $\{n_c t\}$ for which the ground track is tangent to itself at those phase values. Once substituted in Eq. 3.7b), these $\{n_c t\}$ values identify the characteristic inclinations that give the tangency condition (the special case for $n_c t = 0$ can be regarded as a limit). These constitute a set of characteristic inclinations determined by the values of N_p and N_d, andtherefore, they are specific for every orbit. Equation (3.7b) also implies that the characteristic inclinations approach 90° monotonically as $n_c t$ increases. Whether a certain compatible orbit has one or more characteristic inclinations depends on the value of τ. Empirical analysis shows that there will always be at least 2 characteristic inclinations as long as $\tau \geq 5/3$.

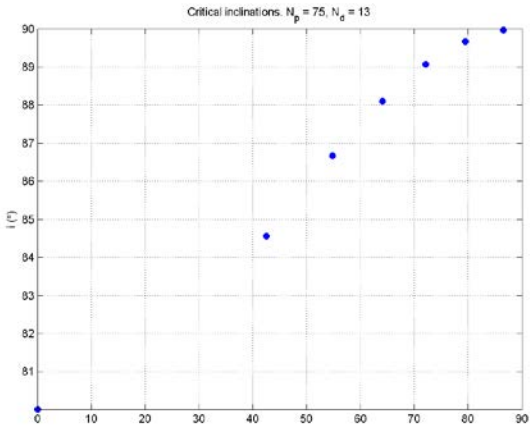

FIGURE 3 CRITICAL INCLINATIONS FOR A COMPATIBLE ORBIT.

As previously discussed, subsequent ground tracks of an orbit inclined at i_1^* with N_p both and N_d odd will be tangent at the equator. If the inclination is equal to i_2^*, then subsequent ground tracks will be tangent at the associated phase value. In general, an orbit at the i_k^* characteristic inclination (with k>2), will have its first-passage ground track tangent to the one corresponding to the k–1 subsequent passage, respectively.

For retrograde orbits ($i > 90°$) the first derivative is positive at both extremes of the interval. Therefore, no stationary points are possible for f, which takes strictly monotonically increasing values in the interval $[(N_p - N_d)/2, N_p]$, and the ground track of a retrograde orbit will never be tangent to itself at any point.

In conclusion, f assumes integer values in the interval $[f_a, f_b]$, according to the following scheme (for the unique case of $N_p = 3$ and $N_d = 2$, i_2^* is not defined and i_1^*has to be used in the formulas instead):

$$\begin{cases} 0 < i < i_2^* & \rightarrow \quad f \in \left[0, \left\lfloor \frac{N_p - N_d}{2} \right\rfloor\right] \\ i_2^* < i < \pi/2 & \rightarrow \quad f \in \left[0, \left\lfloor \max_{n_c t \in [0, \pi/2]} f(n_c t) \right\rfloor\right] \\ i > \pi/2 & \rightarrow \quad f \in \left[\left\lceil \frac{N_p - N_d}{2} \right\rceil, N_p\right] \end{cases}$$

For clarity sake, the results of our analysis are summarized here:

1. Function f assumes integer values in the interval $[\lceil f_{min} \rceil, \lfloor f_{max} \rfloor]$. For prograde orbits, $f_{\min} = 0$, while for retrograde orbits $f_{\min} = (N_p - N_d)/2$.
2. As long as $i < i_1^*$, function f is monotonically decreasing. The greatest integer is equal to $\lfloor (N_p - N_d)/2 \rfloor$.
3. If $N_p - N_d$ is even at the first characteristic inclination, the ground track goes along the local meridian (perpendicular to the equator). Subsequent ground tracks are also tangent there, and for greater inclinations the ground track shows a "reversed" intersection pattern compared to the typical one of lower inclinations, but which keeps the same properties of symmetry and pattern repetition.
4. If $N_p - N_d$ is odd, then subsequent ground tracks will be tangent to each other for the first time at the second characteristic inclination, at the phase $(n_c t)^*$,

$$(n_c t)^* = \frac{1}{\sin i_2^*}\sqrt{\left(1-\frac{N_p}{N_d}\cos i_2^*\right)} \qquad (3.10)$$

that always falls inside the searching interval, and the reversed pattern appears for inclinations greater than i_2^*.

5. As $n_c t$ increases, function f assumes one or more integer values. For each of these values there will be 2 sets of N_p intersections symmetric with respect to the equator, one located along the orbits at phase $(n_c t)^{**}$, and the other at phase $\pi - (n_c t)^{**}$. If the orbit is also inclined at one of the characteristic inclinations associated with the $(n_c t)^{**}$ values then at $(n_c t)^{**}$ the ground track intersects itself with vertical tangent.
6. For retrograde orbits, function f has no stationary points within the interval. The maximum occurs at the right extreme of the interval, where the value is N_p.

Dwell Time Estimation

A first order approximation of the dwell (observation) time of the satellite above a certain intersection point can be obtained. Given the orbit inclination i, the radius r, and setting simplicity $\Omega = 0$, the velocity vector of the satellite in the ECI frame can be easily written as

$$\mathbf{v}_{\text{sat}} = \sqrt{\frac{\mu}{r}} R_1^T(i) \begin{Bmatrix} -\sin(n_c t) \\ \cos(n_c t) \\ 0 \end{Bmatrix}$$

In the ECI frame, the Earth rotational velocity at the given intersection point is

$$\mathbf{v}_{\text{site}} = |\,\boldsymbol{\omega}_\oplus \times (R_\oplus\ \hat{\mathbf{r}}_i)| \begin{Bmatrix} -\sin(\omega_\oplus t) \\ \cos(\omega_\oplus t) \\ 0 \end{Bmatrix} = R_\oplus \omega_\oplus \cos\lambda \begin{Bmatrix} -\sin(\omega_\oplus t) \\ \cos(\omega_\oplus t) \\ 0 \end{Bmatrix}$$

Therefore, the relative velocity between satellite and intersection point can be obtained by simply adding the two vectors

$$\mathbf{v} = \mathbf{v}_{\text{sat}} + \mathbf{v}_{\text{site}} = \sqrt{\frac{\mu}{r}} \begin{Bmatrix} -\sin(n_c t) \\ \cos i \cos(n_c t) \\ \sin i \sin(n_c t) \end{Bmatrix} + R_\oplus \omega_\oplus \cos\lambda \begin{Bmatrix} -\sin(\omega_\oplus t) \\ \cos(\omega_\oplus t) \\ 0 \end{Bmatrix}$$

The magnitude of this vector is

$$v^2 = v_{\text{site}}^2 + v_{\text{sat}}^2[1+\cos(2n_c t)] + 2v_{\text{site}}v_{\text{sat}}[\sin(\omega_\oplus t)\sin(n_c t) + \cos i\cos(\omega_\oplus t)\cos(n_c t)]$$

where $v_{\text{site}} = R_\oplus \omega_\oplus \cos\lambda$ and $v_{sat} = \sqrt{\mu/r}$. As a first approximation, this relative velocity can be assumed constant during the whole observation time. Therefore, given the nominal altitude of the satellite, $h = r - R_\oplus$, the observing sensor field-of-view angle, α, and ignoring the curvature of the Earth, the distance traveled by the satellite while in view of the target can be linearly estimated and consequently, the observation dwell time can be computed, as shown in Fig. 4.

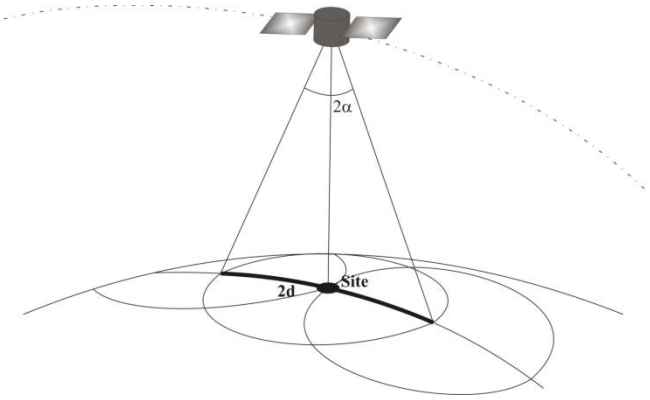

FIGURE 4 SATELLITE PASSAGE ABOVE AN INTERSECTION POINT

In fact, the geometry allows us to write

$$d \approx h\sin\alpha \quad \rightarrow \quad t_{\text{dwell}} = \frac{2d}{v} = \frac{2h\sin\alpha}{v}.$$

Numerical Examples

In the following section we illustrate different possible cases associated with the various behaviors of the parameter f as i increases. For each case, the

intersection pattern both in a 3-D and 2-D view is shown, plus the plot of the parameter f and the passage above a certain intersection point with the associated dwell time.

Case 1 – $i<i_1^*$

This is the case relative to a prograde orbit whose inclination is lower than the characteristic value. The behavior does not change if the sum $N_P + N_d$ is even or odd. The repetition pattern for a resonant orbit with $i < i_1^*$ and ground track are shown in Fig. 5 and Fig. 6, respectively. Figure 7 shows the behavior of the parameter f and Fig. 8 shows the passage of the satellite above an intersecting X-point.

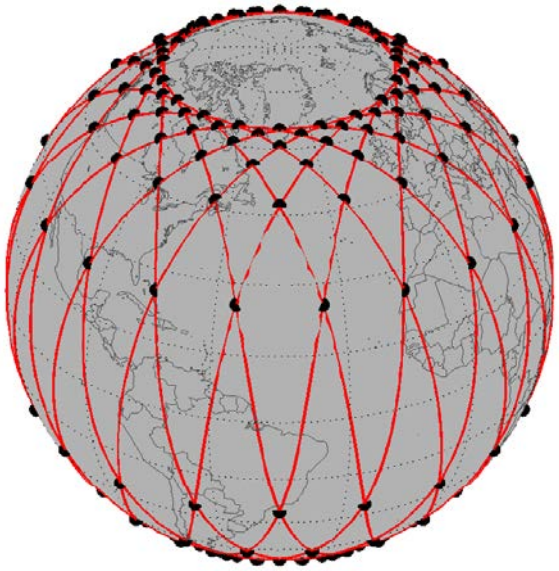

FIGURE 5 3-D VIEW

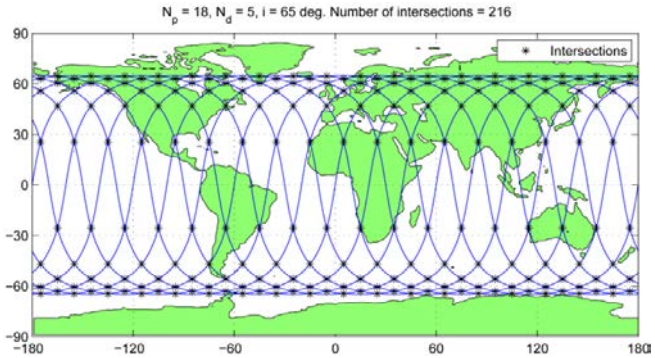

FIGURE 6 2-D VIEW

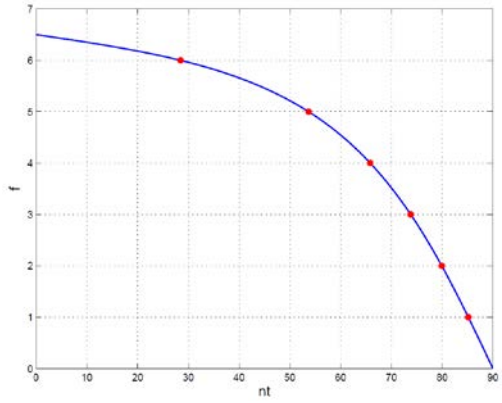

FIGURE 7 PARAMETER f FOR A RESONANT ORBIT WITH $i< i_1^*$

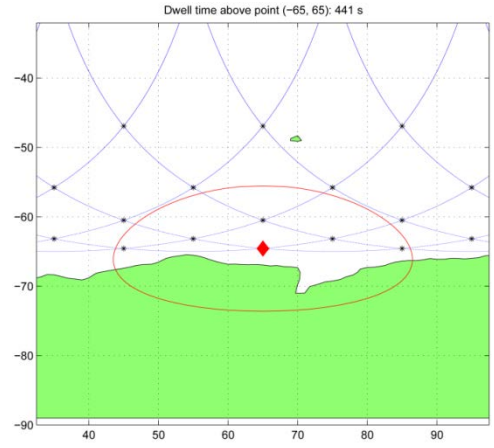

FIGURE 8 DWELL TIME FOR A RESONANT ORBIT WITH $i< i_1^*$

Case 2 - N_P+N_d even, $i \cong i_1^*$

This is the case of an orbit with even $N_P + N_d$, and inclination close to the characteristic value i_1^*. The repetition pattern for a resonant orbit with even $N_P + N_d$ at characteristic inclination is shown in Fig. 9 and Fig. 10, where it is possible to observe how successive tracks are tangent at the equator. Figure 11 shows how the parameter f has a maximum at $n_c t = 0$. The dwell time is shown in Fig. 12.

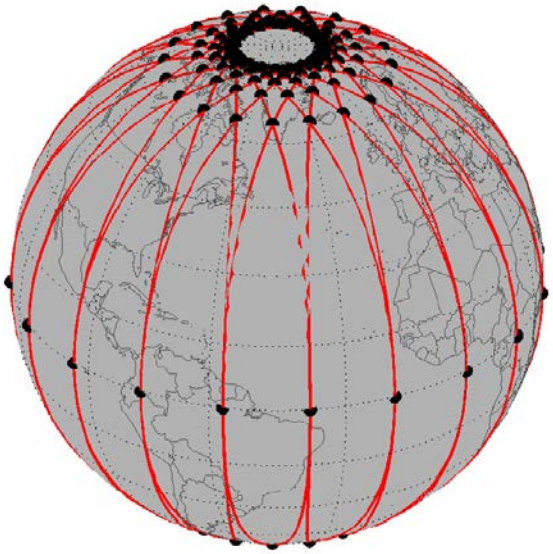

FIGURE 9 3-D VIEW

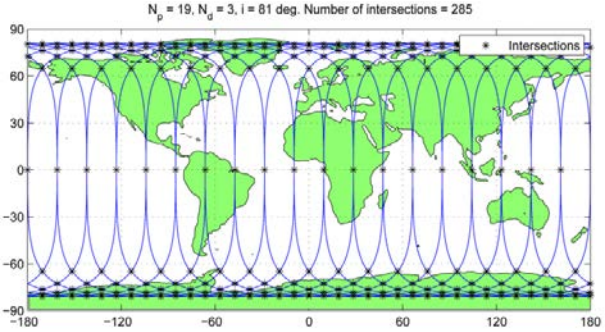

FIGURE 10 2-D VIEW

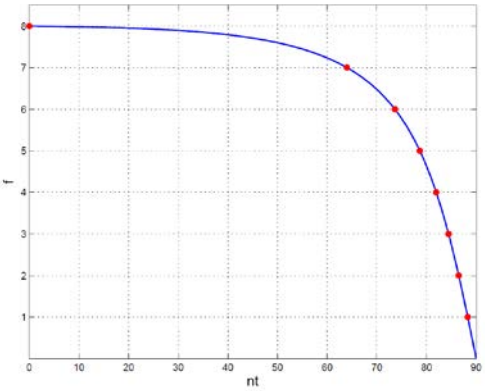

FIGURE 11 PARAMETER f FOR A RESONANT ORBIT WITH N_P + N_d EVEN, AT CHARACTERISTIC INCLINATION

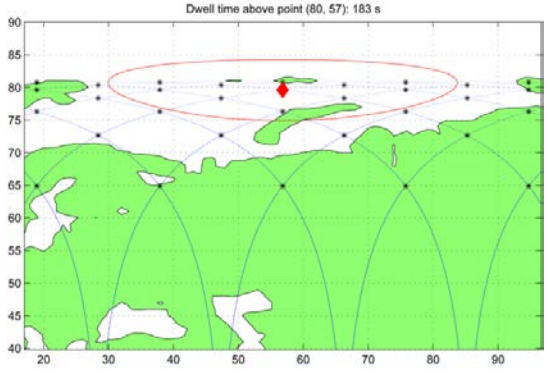

FIGURE 12 DWELL TIME FOR A RESONANT ORBIT WITH N_p + N_d EVEN, AT CHARACTERISTIC INCLINATION

Case 3 - N_p+N_d even, $i \cong i_2^*$

This is the characteristic case for all the orbits with odd N_P + N_d. Repetition pattern for a resonant orbit with odd N_P + N_d at characteristic inclination, is shown in Fig. 13 and Fig. 14, where the tracks are tangent not at the equator, but at two specific latitude values symmetric with respect to the equator itself. It is possible to notice from Fig. 15 how the parameter has its maximum equal to an integer.

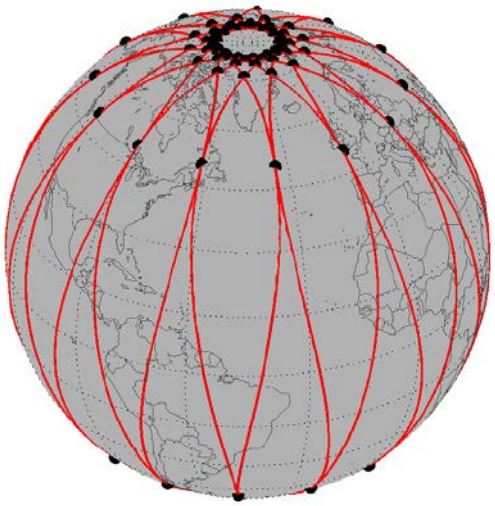

FIGURE 13 3-D VIEW

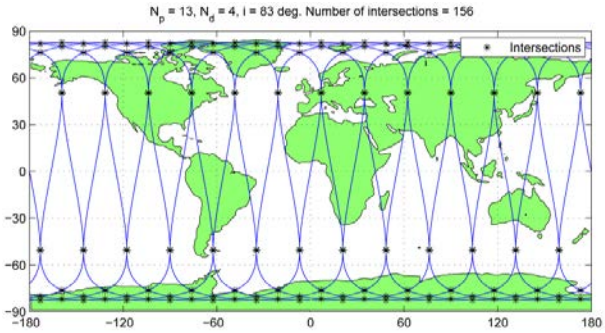

FIGURE 14 2-D VIEW

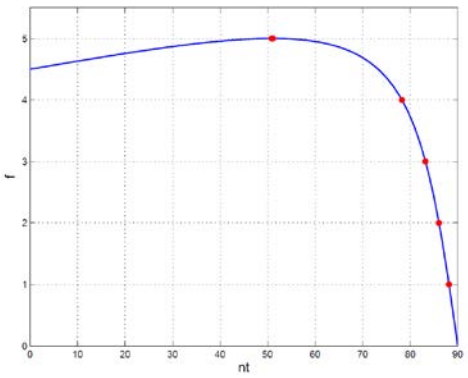

FIGURE 15 PARAMETER f FOR A RESONANT ORBIT WITH N_p + N_d ODD, AT CHARACTERISTIC INCLINATION

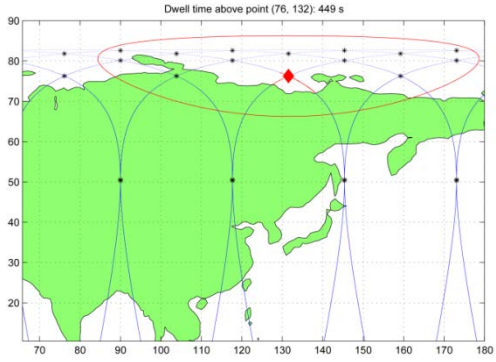

FIGURE 9 DWELL TIME FOR A RESONANT ORBIT WITH $N_p + N_d$ ODD, AT CHARACTERISTIC INCLINATION

Case 4 – i>i*

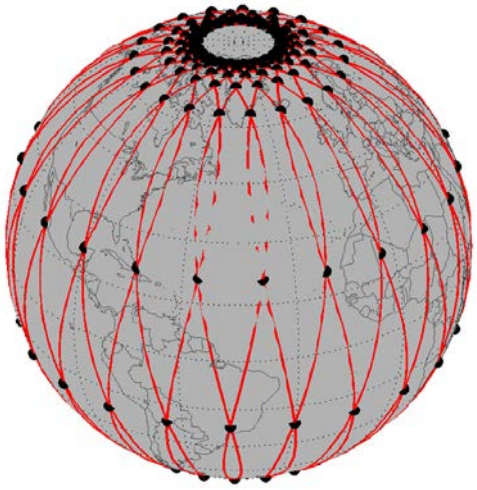

FIGURE 17 3-D VIEW

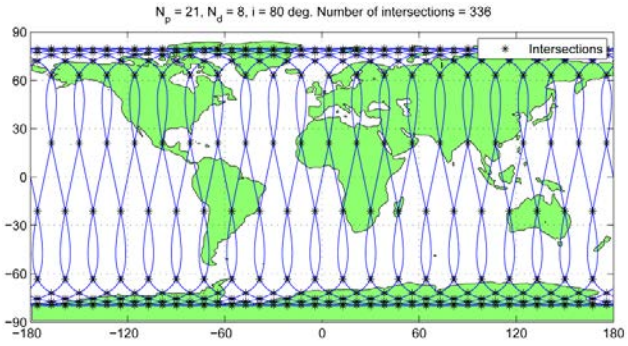

FIGURE 18 2-D VIEW

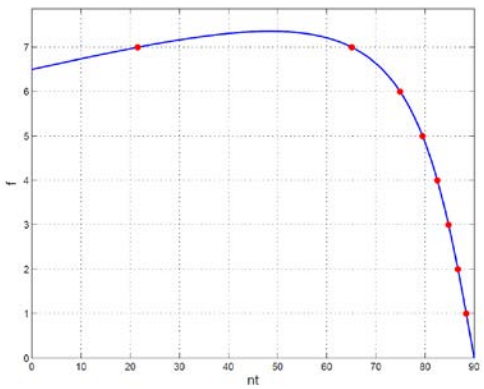

FIGURE 10 PARAMETER *f* FOR A RESONANT ORBIT AT INCLINATION GREATER THAN CHARACTERISTIC

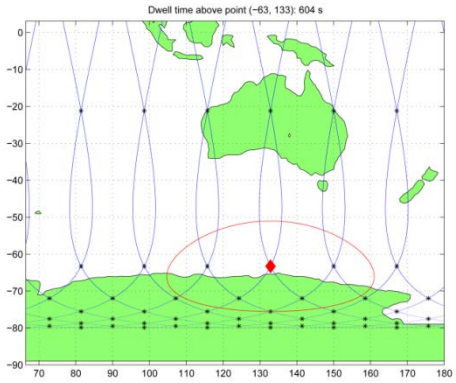

FIGURE 11 DWELL TIME FOR A RESONANT ORBIT AT INCLINATION GREATER THAN CHARACTERISTIC

When the inclination goes beyond the characteristic value, the satellite will move opposite to the Earth rotation, which causes a change in the pattern of intersections. The repetition pattern for a resonant orbit at supercritical inclination is shown in Fig. 17 and Fig. 18. The maximum of *f* increases further and reaches higher integer values, thus new intersections appear (Fig. 19).

Case 5 – i>90°

When the orbit is fully retrograde, the parameter *f* will become monotonically increasing (Fig. 23). The repetition pattern for a resonant retrograde orbit with different type of intersection pattern is shown in Fig. 21 and Fig. 22.

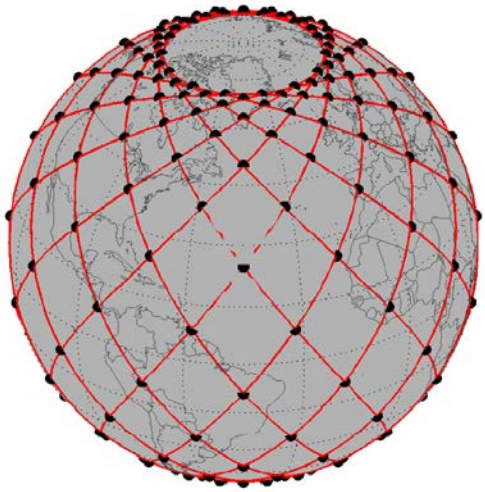

FIGURE 21 3-D VIEW

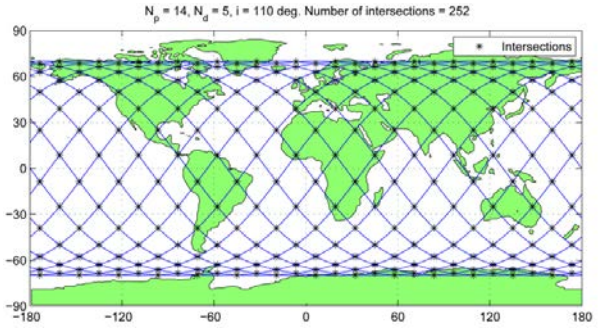

FIGURE 22 2-D VIEW

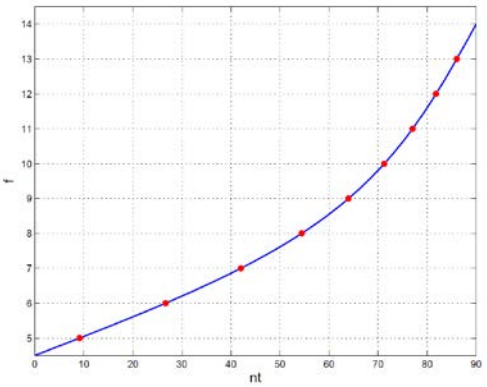

FIGURE 23 PARAMETER *F* FOR A RESONANT RETROGRADE ORBIT

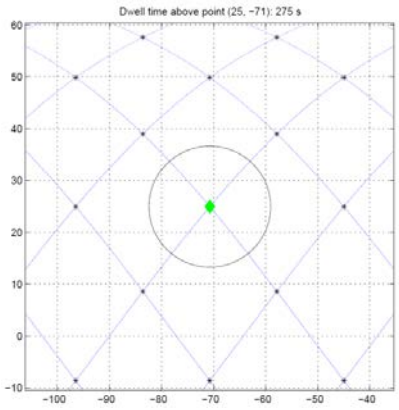

FIGURE 24 DWELL TIME FOR A RESONANT RETROGRADE ORBIT

Conclusions

This study contains analytical equations developed for optimization of satellites and constellations for Earth observation using circular and compatible orbits. Based on intrinsic properties of a repetitive ground track, which presents many intersection points during a repetition period, the relations between the orbit parameters and the coordinates of the *X*-points, are revealed. Therefore, the orbit can be designed to take the biggest possible advantage from the innate symmetry of the intersection pattern. For instance, if a mission requires the satellite to have a *X*-points at certain specific coordinates, the other *X*-points can be used to enhance the scope of the mission, if they happen above other interesting sites. Conversely, if repeated coverage of a certain zone is required, consideration on the dimension of the field of view of the satellite is possible to design the orbit so that the zone is surrounded by the highest possible number of *X*-points which have coverage 2 to 4 times more frequent than that for usual orbits.

AKNOWLEDGEMENTS

This work has been supported by NSF (Grant OISE-I004064).

REFERENCES

LeDrew, Ellsworth F., Wulder, M. and Holden, H. "Change Detection of Satellite Imagery for Reconnaissance of Stressed Tropical Corals" in Proceedings of Geoscience and Remote Sensing Symposium, 2000.

Thomson, M.C. et. al.. "The ecology of malaria as seen from Earth-observation satellites", Annals of Tropical Medicine and Parassitology, pp. 243-264, Liverpool School of Tropical Medicine, U.K, 1996.

Cordeau J.-F. and Laporte G. "Maximizing the value of an Earth observation satellite orbit", Journal of the Operational Research Society, pp.962-968, Montreal, Canada, 2005.

Clay R. "Saving Earth from Space", "Environmental Health Perspectives", vol. 109, pp.A594-A597, 2001.

Kumar, S. and Moore, K.B. "The evolution of Global Positioning System Technology", Journal of Science Education and Technology, Vol. 11, pp. 59-80, 2002.

McGruther, K and Behling, T. "Planning Satellite Reconnaisance to Support Military Operations", Center for the Study of Intelligence, Washington DC, 1999.

Florini, A. "The Opening Skies: Third-Party Imaging Satellites and U.S. Security", International Security , Vol. 13, No. 2 , pp. 91-1231988.

Mortari, Daniele and Abdelkhalic, Ossama. "Two-Way Orbits", Celestial Mechanics and Dynamical Astronomy, pp.399-410, 2006.

Carter, D. "When is the Groundtrack Drift Rate Zero?", Cambridge, 1991.

Wagner, W. E. and Velez, C. E. "Goddard Trajectory Determination Subsystem Mathematical Specifications", NASA Goddard Space Flight Center, 1972.

Francesco de Dilectis was born in Naples, Italy, on the 12th of May 1983. He attended University of Naples "Federico II" in Naples, Italy, where he attained is B.S. (2004) and M.S. (2008) in Aerospace Engineering. He is currently pursuing a Ph.D. in Aerospace Engineering at Texas A&M University. His research interests include celestial mechanics, orbit design and control and satellite dynamics.

Daniele Mortari has received his doctoral degree in Nuclear Engineering from University of Rome "La Sapienza", in 1981.

He is Professor of Aerospace Engineering at Texas A&M University, , working on the field of spacecraft dynamics and control. In addition, he has taught at the School of Aerospace Engineering of Rome's University, and at Electronic Engineering of Perugia's University. He has made contributions in two key areas of specialization: spacecraft attitude and orbit estimation and spacecraft constellations design. His contributions are in both theory and practice. One of his Star-ID algorithms (*Pyramid*) has been widely adopted and recognized as the gold standard for both efficiency and reliability. He also has solved the related problem of determining the best estimate of spacecraft orientation and orbit from vectors observation. In particular, he has developed robust and accurate space-based orbit determination algorithms. Finally, he has developed an entirely new class of spacecraft constellations, the *Flower Constellations*. This opens the new area of shape-preserving constellations and increases the dimensionality of the current solutions for space missions such as global/regional observation, global navigation, communication, and radio occultation. He has published more than 230 papers, holds U.S. patent, and has been widely recognized for his work, including receiving best paper Award from AAS/AIAA, two NASA's Group Achievement Awards, the 2003 Spacecraft Technology Center Award, and the prestigious 2007 IEEE Judith A. Resnik Award.

Dr. Mortari is AAS Fellow, AIAA Associate Fellow, IEEE Senior Member, IEEE Distinguish Speaker, and Honorary Member of IEEE-AESS Space System Technical Panel.